IEEE Access
Multidisciplinary | Rapid Review | Open Access Journal

Received 25 February 2023, accepted 25 March 2023, date of publication 12 April 2023, date of current version 17 August 2023.

Digital Object Identifier 10.1109/ACCESS.2023.3266425

RESEARCH ARTICLE

Single Current Sensor-Based Speed Sensorless Vector Controlled PMSM Drive

SAI SHIVA BADINI[1], VIMLESH VERMA[1], (Senior Member, IEEE), MOHD TARIQ[2], (Senior Member, IEEE), AND SHABANA UROOJ[3], (Senior Member, IEEE)

[1]Department of Electrical Engineering, National Institute of Technology Patna, Patna 800005, India
[2]Department of Electrical Engineering, ZHCET, Aligarh Muslim University, Aligarh 202002, India
[3]Department of Electrical Engineering, College of Engineering, Princess Nourah bint Abdulrahman University, P.O.Box 84428, Riyadh 11671, Saudi Arabia

Corresponding authors: Mohd Tariq (tariq.ee@zhcet.ac.in) and Shabana Urooj (smurooj@pnu.edu.sa)

This work was supported by Princess Nourah bint Abdulrahman University, Riyadh, Saudi Arabia, through the Researchers Supporting Project (PNURSP2023R79).

ABSTRACT Single current sensor-based speed sensorless vector controlled PMSM (''Permanent Magnet Synchronous Motor'') drive is presented in this paper. Speed, position, and currents are estimated using single current sensor information of 3-Φ PMSM drive. 2-Φ currents in the $dq-axes$ are calculated and closed in the loop using i_{qs}^{*} and a phase current information obtained from the single current sensor. The proposed method applies to all types of 3-Φ PMSM; current estimation is independent of machine parameters and inverter switching states. Drive is made speed and position sensorless by estimating using Y-MRAS (Model Reference Adaptive System). Y-MRAS is developed using reference voltages and estimated currents. The speed estimator depends on stator resistance; any variation in it will affect the drive performance. So, stator resistance needs to be estimated online and compensated in the speed estimation technique. Modified P-MRAS technique is used for stator resistance estimation. Here, the drive performance is also validated under stator resistance variation and its compensation. The proposed drive is independent of switching states, integrator terms, and differentiator terms. The single sensor drive reduces the overall cost of the drive and can be implemented into the existing system for sensor condition monitoring and to make the drive fault tolerant against the sensor failure without any extra hardware. The proposed single sensor-based drive is theoretically-modeled and simulated in the MATLAB/SIMULINK platform. The stability of the proposed drive is verified through a stability analysis. It is experimentally validated using a laboratory-developed PMSM drive prototype with a dSPACE-1104 controller board.

INDEX TERMS Estimating—current, speed, position, MRAS, PMSM, single current sensor, speed-sensorless.

NOMENCLATURE

i_{abc}	3-Φ source currents.
$i_{\alpha s}$ & $i_{\beta s}$	Source currents in $\alpha-\beta$ coordinates.
i_{ds}^{*} & i_{qs}^{*}	Reference currents in $d-q$ coordinates.
i_{ds} & i_{qs}	Source currents in $d-q$ coordinates.
$i_{\alpha s-est}$ & $i_{\beta s-est}$	Estimated currents in $\alpha-\beta$ coordinates.
$i_{\alpha s}^{*}$ & $i_{\beta s}^{*}$	Reference currents in $\alpha-\beta$ coordinates.
i_{ds-est} & i_{qs-est}	Estimated currents in $d-q$ coordinates.
v_{ds} & v_{qs}	Source voltage in $d-q$ coordinates.
v_{ds}^{*} & v_{qs}^{*}	Reference voltage in $d-q$ coordinates.
$\omega_{r}^{*}, \omega_{r-est}, \omega_{r}$	Reference, Estimated, and Actual speed.
θ_{s}&θ_{s-est}	Actual and Estimated Position.

The associate editor coordinating the review of this manuscript and approving it for publication was Alfeu J. Sguarezi Filho.

I. INTRODUCTION

The PMSM (Permanent Magnet Synchronous Motors) applications are increased significantly in recent years in Robotics, Electric Vehicles, Machine tools, Industrial drives,

This work is licensed under a Creative Commons Attribution-NonCommercial-NoDerivatives 4.0 License. For more information, see https://creativecommons.org/licenses/by-nc-nd/4.0/

and actuators. PMSM has advantages over the other: higher torque to inertia, compact in size, high efficiency, and power density [1]. The sensor noise will degrade the drive performance; perhaps sensor's failure will lead to drive instability. The accuracy/precision of sensors (i.e., current/speed/position sensors) limits the reliability. So, regular sensor condition monitoring is required.

The majority of vector-controlled PMSM drives now in use include at least two current sensors in addition to a speed/position sensor [1], [2]. Sometimes these sensors may fail or pick up noise or dc offset, which will affect the drive performance [3], [4], [5], [6], [7]. Also, the cost of drive increases with the presence of these sensors. Hence, to reduce the drive cost, increase reliability, and make it fault-tolerant against sensor failure/noise/dc offset, sensorless techniques are preferred for vector-controlled PMSM drive. By using the speed/current estimation approaches in open loop, sensor condition monitoring and fault-tolerant operation can be performed [4], [6], [8], [9], [10], [11], [12], [13], [14], [15], [16], [17], [18], [19], [20], [21], [22].

A single current sensor-based speed sensorless vector control PMSM drive is suggested in this study to reduce the number of sensors used in the drive. i.e., speed sensor & one current sensor are eliminated. A single current sensor drive increases reliability and stability. Some of the single current sensor-based approaches for PMSM drive presented in the literature are [9], [10], [11], [12], [21], and [23]. A brief literature study on the various current and speed estimation techniques is discussed and followed by the proposed drive in this section. Based on the placement of the current sensor, the reconstruction of three-phase currents is divided into DC link current measurement, Multiple branch current measurements with a single current sensor, and single-phase current measurement [10], [12], [22], [24], [25], [26], [27], [28], [29], [30], [31], [32], [33], [34], [35]. In multiple branch current measurement methods, the current sensor is employed to measure more than the rated current, which increases the current sensor's cost.

In [12], [22], [23], [36], and [37], using inverter switching information and DC link current: 3-Φ currents are reconstructed. Although it is a common strategy, it has the following limitations [25], [26], [35], [38]: (a) phase variation in predicted currents, (b) short duration of active-switching states/near the sector boundary, and (c) a low-modulation index. Using a single DC current sensor, some techniques are reported in the literature that addresses the shortcoming of existing methods while also introducing new strategies for enhancing the accuracy in the reconstruction of phase currents in all regions [11], [28], [39]. An isolated current sensor topology detects currents corresponding to the DC link in the zero voltage vector sampling zone [10].

The problem associated with the short duration of switching states is overcome using the measurement vector insertion method [40]. Measuring phase currents under the sector boundary region conditions/low modulation index is presented in [26]. However, these approaches rely on inverter switching states and DC link current, which need huge analysis for phase current reconstruction. Many articles are presented in the literature on single current sensor approach drive, and few are presented here [41], [42], [43], [44], [45]. Most of the single current sensor-based systems depend on a current sensor to measure DC link current and to reconstruct phase currents; signal-injection/observer-based methodologies are used to estimate speed.

In [46], the observer design approach is implemented using a current sensor to reconstruct the remaining phase currents. However, this is dependent on machine parameters and involves phase voltages. In [9], the currents are estimated in $dq-axes$ 2-Φ currents quantities. The rotor reference frame 2-Φ currents are estimated from current sensor information and the q-axes reference current. The present estimation method is not affected by the change in machine parameters. To overcome the drawbacks of current reconstruction/estimation methodologies, this paper presents a two-phase rotor reference frame current estimation strategy based on single-phase current sensor information. the proposed current estimation is independent of machine parameters, switching states integrator and differentiator.

Further, the speed/position is also eliminated and replaced with the estimation technique. In the literature [1], [47], [48], [49], [50], [51], [52], [53], [54], [55], [56] present the speed sensorless PMSM drive. Back EMF (e), State Observer (SO), Model-based approaches, Signal Injection (SI), and others like Artificial-Intelligence (AI) are some of the categories (AI). The Back-EMF-based speed estimate approaches function better at mid to highs, but they cannot track back-emf at zero speeds. It makes the estimation technique extremely tough.

The SI-based approach operates well at zero speed. The primary disadvantage of SI-based solutions is the negative effect of SI on motor dynamics. The need for additional hardware for SI adds to the drive cost. Observer-based approaches are sensitive to machine parameters, need filters and initial conditions, and involve complex mathematics analysis. Combining "e" with "SI"-based approaches yields superior performance across a wide range of operations.

MRAS computes 2-functional candidates stated in distinct equations with the same quantity. Both the adjustable and reference models are used to produce an error that passes through PI and is closed to the adjustable model until the error is zero [47], [54], [57], [58]. MRAS based approch performs satisfactory performance from high speed range to zero speeds also [53], [58], [59], [60], [61], [62], and [63]. Other methods, such as AI, fuzzy, ANN, etc., [48], [56], [64], and [65] are modern approaches that need a large amount of data to train the system and are more difficult to implement. In the study, the MRAS-based ω_r estimation approach is applied to build the drive speed sensorless. The following features make MRAS-based techniques more attractive: simplicity, stability, no Extra-Hardware, reduced computation-complexity, independent of integrator, and differentiation terms.

Using the proposed current estimation technique and Y-MRAS-based speed estimation technique makes the drive work with only one sensor (i.e., only one current sensor). The speed/current estimation techniques can be used to monitor the status of sensors (i.e., speed and current) by implimenting in the existing PMSM drive. No additional hardware is required to implement the proposed single current sensor-based vector-controlled PMSM drive. Implementing a single sensor-based drive can reduce the cost of the drive, complexity in the system, increases the reliability and immunity to signal noise as only one current sensor is used.

The Modeling of PMSM is presented in Section II. Section III discusses the mathematical analysis for current and speed estimation techniques. Section IV presents the stability analysis for the proposed drive. MATLAB/Simulation outcomes for the presented techniques are shown in Section V. Experimental validation and outcomes are presented and explained in Section VI. Section VII conclude the work.

II. PMSM MODELING

The stator voltage in the "$dq - axes$" rotor reference frame for PMSM are shown in (1). The PMSM machine modeling is taken from [1].

$$\begin{pmatrix} v_{ds} \\ v_{qs} \end{pmatrix} = \begin{bmatrix} R_s + L_d Þ & -\omega_s L_q \\ \omega_s L_d & R_s + L_q Þ \end{bmatrix} \begin{pmatrix} i_{ds} \\ i_{qs} \end{pmatrix} + \begin{pmatrix} 0 \\ \omega_s \lambda_{af} \end{pmatrix} \tag{1}$$

$$T_e = \left(\frac{3}{2}\right) P i_{qs} \left(L_d - L_q\right) i_{ds} + \lambda_{af} \tag{2}$$

$$T_e - T_L = J Þ \omega + B \omega_r \tag{3}$$

Electrical torque developed in the machine is shown in (2). Equation (3) presents the electro-mechanical dynamics equation where electric and load-torque are T_e and T_L, respectively. $Þ$ = derivativeterm ($\frac{d}{dt}$), $P = polepair$, ω_s, &ω_r are synchronous speed & rotor speed ($\omega_s = P\omega_r$), R_s = stator resistance.

III. ESTIMATION TECHNIQUES

A. CURRENT ESTIMATION TECHNIQUE

The current sensor is attached to any one of the motor phases and is referred as phase-A in this context. Clark's transformation is used to compute the α-axes current from the phase-A current. As a result, under-balanced circumstances (10) is obtained.

$$\begin{pmatrix} i_{\alpha s} \\ i_{\beta s} \end{pmatrix} = \sqrt{\frac{2}{3}} \begin{pmatrix} 1 & -0.5 & -0.5 \\ 0 & \frac{\sqrt{3}}{2} & -\frac{\sqrt{3}}{2} \end{pmatrix} \begin{pmatrix} i_a \\ i_b \\ i_c \end{pmatrix} \tag{4}$$

$$i_{\alpha s} = \sqrt{\frac{2}{3}} (i_a - 0.5\,(i_b + i_c)) \tag{5}$$

Under, 3-Φ balanced current condition:

$$i_a + i_b + i_c = 0 \tag{6}$$

$$i_b + i_c = -i_a \tag{7}$$

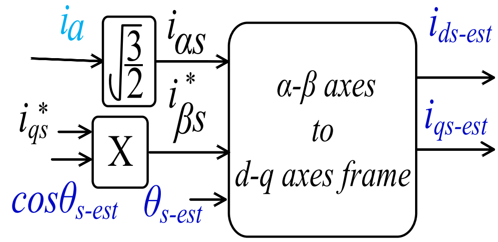

FIGURE 1. Block diagram presents the current estimating technique.

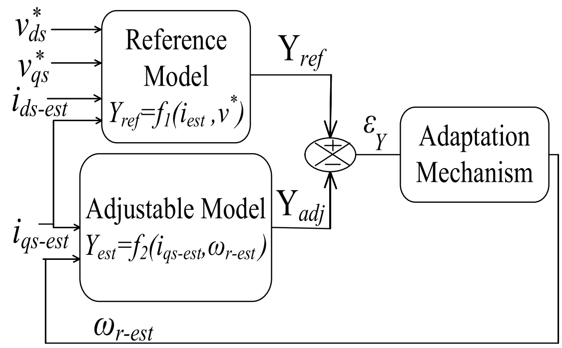

FIGURE 2. MRAS structure for speed estimation.

Substituting (7) in (4), $i_{\alpha s}$ becomes:

$$i_{\alpha s} = \sqrt{\frac{2}{3}} (i_a - \frac{1}{2}(-i_a)) \tag{8}$$

$$i_{\alpha s} = \sqrt{\frac{2}{3}} (\frac{3}{2}(i_a)) \tag{9}$$

$$i_{\alpha s} = \sqrt{\frac{3}{2}} (i_a) \tag{10}$$

The reference currents in the β-axes is formulated using inverse Park's transformation from $dq - axes$ reference currents. estimated (θ_{s-est})/Actual (θ_s) position obtained from the Estimated (ω_{r-est})/Actual (ω_r) speed. $i^*_{ds} = 0$ is maintained in vector-controlled PMSM drive.

$$\begin{pmatrix} i^*_{\alpha s} \\ i^*_{\beta s} \end{pmatrix} = \begin{pmatrix} \cos\theta_s & -sin\theta_s \\ \sin\theta_s & \cos\theta_s \end{pmatrix} \begin{pmatrix} i^*_{ds} \\ i^*_{qs} \end{pmatrix} \tag{11}$$

$$i^*_{\beta s} = i^*_{qs} cos\theta_s \tag{12}$$

$$\theta_s = \int \omega_s dt = P \int \omega_r dt \tag{13}$$

The $\alpha\beta$-axes currents (i.e., $i_{\alpha s}$ and $i^*_{\beta s}$ from (10) and (12)) are transformed into $dq - axes$ currents by using the park's transformation. As shown in Fig. 1, the predicted $dq - axes$ currents are employed to complete the closed-loop control.

$$\begin{pmatrix} i_{ds-est} \\ i_{qs-est} \end{pmatrix} = \begin{pmatrix} \cos\theta_s & \sin\theta_s \\ -sin\theta_s & \cos\theta_s \end{pmatrix} \begin{pmatrix} i_{\alpha s} \\ i^*_{\beta s} \end{pmatrix} \tag{14}$$

$$i_{ds-est} = \left(\sqrt{\frac{3}{2}} i_a + i^*_{qs} \sin\theta_s \right) \cos\theta_s \tag{15}$$

$$i_{qs-est} = -\sqrt{\frac{3}{2}} i_a \sin\theta_s + i^*_{qs} cos^2\theta_s \tag{16}$$

The estimation of $dq - axes$ 2-Φ currents from $i_{\alpha s}$ and $i^*_{\beta s}$ involves rotor position information attained from the speed/position-sensor/estimation.

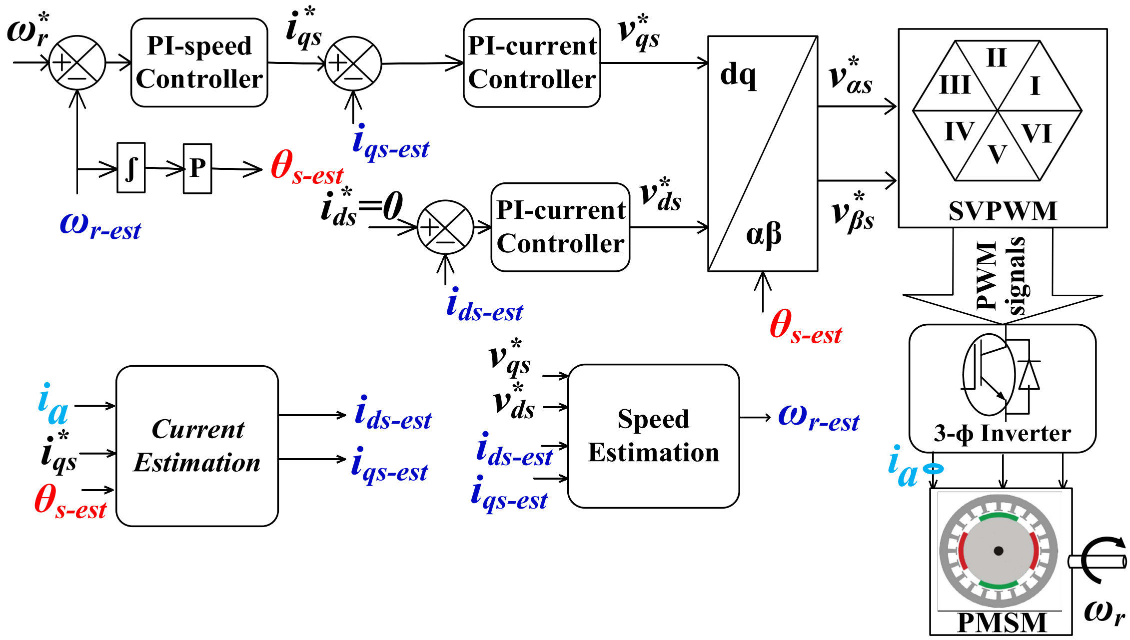

FIGURE 3. Block diagram for single current Sensor-based speed sensorless vector controlled PMSM drive.

A current sensor is connected to any one of the motor phase terminals and referred to phase A and converted to the 2-Φ stationary $\alpha\beta-axes$ reference frame ($i.e., i_{\alpha s}$) from (10). i^*_{qs} is converted to 2-Φ stationary $\alpha\beta$-axes reference frame current $i^*_{\beta s}$ from (12) by using position sensor information. Further, the sensors are reduced in the drive; the speed/position sensor is removed, and the information is replaced with the estimated information. $'\alpha\beta'$ currents ($i_{\alpha s}$ *and* $i^*_{\beta s}$ from (10) and (12)) are converted to the rotor reference frame currents ($d-$ *and* $q-axes$ currents) using the estimated rotor position from (14). The current loop is closed with the estimated currents. The current estimation method is independent of switching states and machine parameters. The remaining phase currents are estimated without any complex analysis from this approach.

B. SPEED ESTIMATION TECHNIQUE

The drive is made speed-sensorless with speed estimation method, by using P [66], Q [54], [67], Y [47], and X [59], [67]. All the estimation techniques perform well under all four quadrant operations. There is no particular advantage of Y-MRAS.in this paper, Y-MRAS is considered for speed estimation technique; which is built from the product of $\vec{v}^*_s$ and $\vec{i}_s$. The Adjustable-Model is reliant on unknown-quantity ω_r($i.e. shaft speed$), where as The Reference-Model is independent of the speed. Error (ε) is formed from the difference between reference and adjustable model quantity. ε produced from reference and adjustable quantities passed through the $PI-Controller$ (i.e., Adaption-Mechanism). The output of adaption mechanism (i.e., $\omega_s = P\omega_r$) is used to tune the adjustable-model; this continues till $\varepsilon_y = 0$.

Apart from Y-MRAS, any other speed estimation technique independent of stator resistance can be used. This will make the drive completely independent of stator resistance. This eliminates the requirement of any R_s estimation. This reduces the complexity of the drive.

The expression for adjustable and reference model for MRAS is considered form [47], [54], [66], and [68]. The Fictitious-Quantity (Y) is expressed in (17) with reference voltages and estimated currents as shown in (21). Substituting (1) in (17); Under steady-state condition: $\frac{d}{dt} = 0$, and the condition for vector control is "i^*_{ds} maintained 0" (i.e., field producing component current =0 A):

$$Y_1 = v_{qs}i_{qs} - v_{ds}i_{ds} \tag{17}$$

$$Y_2 = R_s i^2_{qs} - R_s i^2_{ds} + L_q i_{qs} \text{Þ} i_{qs} - L_d i_{ds} \text{Þ} i_{ds} + \omega_s i_{qs} i_{ds} L_d + \omega_s i_{qs} i_{ds} L_q + \omega_s i_{qs} \lambda_{af} \tag{18}$$

Under steady-state condition: $\frac{d}{dt} = 0$, Y_2 becomes:

$$Y_3 = R_s\left(i^2_{qs} - i^2_{ds}\right) + \omega_s i_{qs} i_{ds}\left(L_d + L_q\right) + \omega_s i_{qs}\lambda_{af} \tag{19}$$

The condition for vector-control is "i_{ds} =0"; Y_3 becomes:

$$Y_4 = R_s i^2_{qs} + \omega_s i_{qs}\lambda_{af} \tag{20}$$

For Reference-Model: Y_1 considered which is independent of ω_s and for the Adjustable-Model: Y_4 is considered which is reliant on on ω_s. The error ($\varepsilon_y = (17) - (20)$) is formulated and sent through Adaption-Mechanism (PI-Controller). Here in Eq. 20, ω_{r-est} (estimated speed) is used instead of ω_r (actual speed). MRAS structure is used for the speed estimation technique shown in Fig. 2. The reference voltages and estimated currents are used in the (17), estimated current, and estimated speed is used in (20) this results in (21) and (22).

$$Y_1 = v^*_{qs} i_{qs-est} - v^*_{ds} i_{ds-est} \tag{21}$$

$$Y_4 = R_s i^2_{qs-est} + \omega_{s-est} i_{qs-est}\lambda_{af} \tag{22}$$

$$\varepsilon_y = Y_1 - Y_4 \tag{23}$$

$$\omega_{\mathrm{r-est}} = k_p * \varepsilon_y + k_i * \int_0^t \varepsilon_y dt + \omega_{\mathrm{r-est}}(0) \tag{24}$$

$$\theta_{s-est} = P\theta_{r-est} = \int \omega_{\mathrm{s-est}} dt = P \int \omega_{\mathrm{r-est}} dt \tag{25}$$

The estimated position is shown in (25) is used in the current estimation technique and the equations are modified.

IV. STABILITY ANALYSIS

The small-signal stability analysis is presented under steady-state for a single current sensor-based speed sensorless vector controlled PMSM drive. PMSM modeling is presented in (26) in rotating reference frame [47], [67], [69].

$$\begin{bmatrix} \dot{ds} \\ \dot{qs} \end{bmatrix} = \begin{bmatrix} \frac{-R_s}{L_d} & \frac{\omega_s L_q}{L_d} \\ \frac{-\omega_s L_d}{L_q} & \frac{-R_s}{L_q} \end{bmatrix} \begin{pmatrix} i_{ds} \\ i_{qs} \end{pmatrix} + \begin{bmatrix} \frac{1}{L_d} & 0 \\ 0 & \frac{1}{L_q} \end{bmatrix} \begin{pmatrix} v_{ds} \\ v_{qs} \end{pmatrix} + \begin{bmatrix} 0 \\ \frac{-\omega_s \lambda_{af}}{L_q} \end{bmatrix} \tag{26}$$

$$\begin{pmatrix} i_{ds} \\ i_{qs} \end{pmatrix} = \begin{bmatrix} 1 & 0 \\ 0 & 1 \end{bmatrix} \begin{pmatrix} i_{ds} \\ i_{qs} \end{pmatrix} \tag{27}$$

In (26) and (27), the state variables are the stator currents in d and q-reference frame. The general form of state-space representation is:

$$\dot{x} = Ax + Bu + E \tag{28}$$

$$y = Cx + Du \tag{29}$$

Comparing (26)-(29), We get.

$$\left.\begin{aligned} A &= \begin{bmatrix} \frac{-R_s}{L_d} & \frac{\omega_s L_q}{L_d} \\ \frac{-\omega_s L_d}{L_q} & \frac{-R_s}{L_q} \end{bmatrix}, \\ B &= \begin{bmatrix} \frac{1}{L_d} & 0 \\ 0 & \frac{1}{L_q} \end{bmatrix}, C = \begin{bmatrix} 1 & 0 \\ 0 & 1 \end{bmatrix} \\ E &= \begin{bmatrix} 0 \\ \frac{-\omega_s \lambda_{af}}{L_q} \end{bmatrix}, y = x = \begin{bmatrix} i_{ds} \\ i_{qs} \end{bmatrix}, D = 0 \\ u &= \begin{pmatrix} v_{ds} \\ v_{qs} \end{pmatrix} = \begin{pmatrix} r_3\left(i_{ds}^* - i_{ds}\right) \\ r_2\left(i_{qs}^* - i_{qs}\right) \end{pmatrix} \\ &= \begin{pmatrix} r_3(i_{ds}^* - i_{ds}) \\ r_2(r_1(\omega_{ref} - \omega_r^*) - i_{qs}) \end{pmatrix} \end{aligned}\right\} \tag{30}$$

where,

$$\left.\begin{aligned} r_1 &= \frac{sk_{p1} + k_{i1}}{s}, r_2 = \frac{sk_{p2} + k_{i2}}{s}, \\ r_3 &= \frac{sk_{p3} + k_{i3}}{s}, r_4 = \frac{sk_{p4} + k_{i4}}{s} \end{aligned}\right\} \tag{31}$$

These $r_{n(n=1,2,3\&4)}$ are the transfer function of the PI- controller speed, PI- controller of q-axes current, PI- controller of d-axes current, and adaptation mechanism in Y-*MRAS*, respectively.

$$y = \begin{pmatrix} i_{ds} \\ i_{qs} \end{pmatrix} \tag{32}$$

Using the small-signal analysis with respect to $'x_0'$ operating point. (28) and (29) become:

$$\dot{\Delta x} = A\Delta x + \Delta A x_0 + B\Delta u + \Delta E \tag{33}$$

$$\Delta y = C\Delta x \tag{34}$$

Taking Laplace-transformation and substituting (33) into (34)

$$\Delta y = C(sI - A)^{-1} \left[\Delta A x_0 + B\Delta u + \Delta E\right] \tag{35}$$

where,

$$\left.\begin{aligned} x_0 &= \begin{pmatrix} i_{ds0} \\ i_{qs0} \end{pmatrix}, \\ \Delta u &= \begin{pmatrix} \Delta v_{ds} \\ \Delta v_{qs} \end{pmatrix} = \left(\begin{pmatrix} -r_3 \Delta i_{ds} \\ -r_2 \Delta i_{qs} - r_1 r_2 \Delta \omega_r \end{pmatrix}\right), \\ \Delta y &= \begin{pmatrix} \Delta i_{ds} \\ \Delta i_{qs} \end{pmatrix}, \\ \Delta E &= \begin{pmatrix} 0 \\ \frac{-\Delta \omega_r P \lambda_{af}}{L_q} \end{pmatrix}, \\ \Delta A &= \begin{bmatrix} 0 & \frac{L_q}{L_d} \\ \frac{-L_d}{L_q} & 0 \end{bmatrix} \Delta \omega_s \end{aligned}\right\} \tag{36}$$

Substituting the values of A, B, C, ΔA, Δu, $\Delta E \& x_0$ in (35), and we obtain the expression for $\left(\frac{\Delta i_{qs}}{\Delta \omega_r}\right)$ and $\left(\frac{\Delta i_{ds}}{\Delta \omega_r}\right)$.

Using small-signal analysis with respect to $'x_0'$ operating point, the expressions for Δi_{qs}^*, Δi_a, Δi_{ds-est} and Δi_{qs-est} become

A. i_{qs}^* IS EXPRESSED AS

$$i_{qs}^* = r_1(\omega_r^* - \omega_{r-est}) \tag{37}$$

$$\Delta i_{qs}^* = \Delta r_1(\omega_r^* - \omega_{r-est}) \tag{38}$$

$$\Delta i_{qs}^* = r_1(0 - \Delta\omega_{r-est}) \tag{39}$$

$$\Delta i_{qs}^* = -r_1 \Delta\omega_{r-est} \tag{40}$$

B. A-PHASE CURRENT IS EXPRESSED IN DQ-AXES CURRENTS

$$i_a = \sqrt{\frac{2}{3}}(i_{ds}\cos\theta_s - i_{qs}\sin\theta_s) \tag{41}$$

As a small perturb is considered in speed results in a negligible amount of change in θ_s. So, $\Delta\theta_s$ is neglected.

$$\Delta i_a = \sqrt{\frac{2}{3}}(\cos\theta_s \Delta i_{ds} - \sin\theta_s \Delta i_{qs}) \tag{42}$$

C. D-AXES ESTIMATED CURRENT IS

$$i_{ds-est} = (\sqrt{\frac{3}{2}} i_a + i_{qs}^{*} \sin\theta_s)\cos\theta_s \tag{43}$$

$$\Delta \mathrm{i}_{\mathrm{ds-est}} = (\sqrt{\frac{3}{2}} \Delta i_a + \sin\theta_s \Delta i_{qs}^{*})\cos\theta_s \tag{44}$$

Further modified by substituting Δi_a in $\Delta \mathrm{i}_{\mathrm{ds-est}}$, we get

$$\begin{aligned}\Delta \mathrm{i}_{\mathrm{ds-est}} &= (\sqrt{\frac{3}{2}}(\sqrt{\frac{2}{3}}(\cos\theta_s \Delta i_{ds} - \sin\theta_s \Delta i_{qs})) \\ &\quad + \sin\theta_s \Delta i_{qs}^{*})\cos\theta_s\end{aligned} \tag{45}$$

By substituting $\frac{\Delta i_{qs}^{*}}{\Delta \omega_{\mathrm{r}}}$, we get

$$\begin{aligned}\Delta \mathrm{i}_{\mathrm{ds-est}} &= (\sqrt{\frac{3}{2}}(\sqrt{\frac{2}{3}}(\cos\theta_s \Delta i_{ds} - \sin\theta_s \Delta i_{qs})) \\ &\quad + \sin\theta_s(-\mathrm{r}_1 \Delta\omega_{r-est}))\cos\theta_s\end{aligned} \tag{46}$$

$$\begin{aligned}\Delta \mathrm{i}_{\mathrm{ds-est}} &= \cos^2\theta_s \Delta i_{ds} - \cos\theta_s \sin\theta_s \Delta i_{qs} \\ &\quad - \cos\theta_s \sin\theta_s \mathrm{r}_1 \Delta\omega_{r-est}\end{aligned} \tag{47}$$

D. Q-AXES ESTIMATED CURRENT IS

$$i_{qs-est} = -\sqrt{\frac{3}{2}} i_a \sin\theta_s + i_{qs}^{*} cos^2\theta_s \tag{48}$$

$$\Delta \mathrm{i}_{\mathrm{qs-est}} = -\sqrt{\frac{3}{2}} \sin\theta_s \Delta i_a + cos^2\theta_s \Delta i_{qs}^{*} \tag{49}$$

Further modified by substituting Δi_a in $\Delta \mathrm{i}_{\mathrm{qs-est}}$, we get

$$\begin{aligned}\Delta \mathrm{i}_{\mathrm{qs-est}} &= -\sqrt{\frac{3}{2}} \sin\theta_s(\sqrt{\frac{2}{3}}(\cos\theta_s \Delta i_{ds} - \sin\theta_s \Delta i_{qs})) \\ &\quad + cos^2\theta_s \Delta i_{qs}^{*}\end{aligned} \tag{50}$$

By substituting $\frac{\Delta i_{qs}^{*}}{\Delta \omega_{\mathrm{r}}}$, we get

$$\begin{aligned}\Delta \mathrm{i}_{\mathrm{qs-est}} &= -\sqrt{\frac{3}{2}} \sin\theta_s(\sqrt{\frac{2}{3}}(\cos\theta_s \Delta i_{ds} - \sin\theta_s \Delta i_{qs})) \\ &\quad + cos^2\theta_s(-\mathrm{r}_1 \Delta\omega_{r-est})\end{aligned} \tag{51}$$

$$\begin{aligned}\Delta \mathrm{i}_{\mathrm{qs-est}} &= -\sin\theta_s \cos\theta_s \Delta i_{ds} + \sin^2\theta_s \Delta i_{qs} \\ &\quad - cos^2\theta_s \mathrm{r}_1 \Delta\omega_{r-est}\end{aligned} \tag{52}$$

E. ERROR FORMED IN MRAS

From (23), the error of the rotor-speed estimation is given by

$$\varepsilon = Y_1 - Y_4 \tag{53}$$

where Y_4 *and* Y_1 are steady-state and instantaneous Fictitious Quantities. The stability analysis is carried out in the rotor reference frame (d and q-axes frame). Both the quantities are expressed in the rotating reference frame.

$$\begin{aligned}\varepsilon &= (v_{qs} i_{qs-est} - v_{ds} i_{ds-est}) \\ &\quad - \left(\mathrm{R}_s i_{qs-est}^2 + P\omega_{r-est} i_{qs-est} \lambda_{af}\right)\end{aligned} \tag{54}$$

$$\begin{aligned}\varepsilon &= v_{qs} i_{qs-est} - v_{ds} i_{ds-est} \\ &\quad - \mathrm{R}_s i_{qs-est}^2 - P\omega_{r-est} i_{qs-est} \lambda_{af}\end{aligned} \tag{55}$$

Considering a small-perturb in ε. $\Delta\varepsilon$ can be expressed as

$$\begin{aligned}\Delta\varepsilon &= v_{qs} \Delta i_{qs-est} - v_{ds} \Delta i_{ds-est} - 2\mathrm{R}_s i_{qs-est} \Delta i_{qs-est} \\ &\quad - P i_{qs-est} \lambda_{af} \Delta\omega_{r-est} - \omega_{r-est} P \lambda_{af} \Delta i_{qs-est}\end{aligned} \tag{56}$$

Dividing the Eq. 54 by $\Delta\omega_r$, we obtain

$$\begin{aligned}\frac{\Delta\varepsilon}{\Delta\omega_r} &= v_{qs}\frac{\Delta i_{qs-est}}{\Delta\omega_r} - v_{ds}\frac{\Delta i_{ds-est}}{\Delta\omega_r} \\ &\quad - 2\mathrm{R}_s i_{qs-est}\frac{\Delta i_{qs-est}}{\Delta\omega_r} - P i_{qs-est}\lambda_{af}\frac{\Delta\omega_{r-est}}{\Delta\omega_r} \\ &\quad - \omega_{r-est} P\lambda_{af}\frac{\Delta i_{qs-est}}{\Delta\omega_r}\end{aligned} \tag{57}$$

$$\begin{aligned}\frac{\Delta\varepsilon}{\Delta\omega_r} &= (v_{qs} - 2\mathrm{R}_s i_{qs-est} - \omega_{r-est} P\lambda_{af})\frac{\Delta i_{qs-est}}{\Delta\omega_r} \\ &\quad - P i_{qs-est}\lambda_{af}\frac{\Delta\omega_{r-est}}{\Delta\omega_r} - v_{ds}\frac{\Delta i_{ds-est}}{\Delta\omega_r}\end{aligned} \tag{58}$$

Substituting $\frac{\Delta \mathrm{i}_{\mathrm{qs-est}}}{\Delta\omega_{\mathrm{r}}}$ and $\frac{\Delta \mathrm{i}_{\mathrm{ds-est}}}{\Delta\omega_{\mathrm{r}}}$ in above equation

$$\begin{aligned}\frac{\Delta\varepsilon}{\Delta\omega_r} &= \left(v_{qs} - 2\mathrm{R}_s i_{qs-est} - \omega_{r-est} P\lambda_{af}\right) \\ &\quad \times (\sin^2\theta_s\frac{\Delta i_{qs}}{\Delta\omega_{\mathrm{r}}} - \sin\theta_s\cos\theta_s\frac{\Delta i_{ds}}{\Delta\omega_{\mathrm{r}}} \\ &\quad - cos^2\theta_s \mathrm{r}_1\frac{\Delta\omega_{r-est}}{\Delta\omega_r}) - P i_{qs-est}\lambda_{af}\frac{\Delta\omega_{r-est}}{\Delta\omega_r} \\ &\quad - v_{ds}(\cos^2\theta_s\frac{\Delta i_{ds}}{\Delta\omega_{\mathrm{r}}} - \cos\theta_s\sin\theta_s\frac{\Delta i_{qs}}{\Delta\omega_{\mathrm{r}}} \\ &\quad - \cos\theta_s\sin\theta_s \mathrm{r}_1\frac{\Delta\omega_{r-est}}{\Delta\omega_r})\end{aligned} \tag{59}$$

$$\begin{aligned}\frac{\Delta\varepsilon}{\Delta\omega_r} &= \left(v_{qs} - 2\mathrm{R}_s i_{qs-est} - \omega_{r-est} P\lambda_{af}\right) \\ &\quad \times (\sin^2\theta_s\frac{\Delta i_{qs}}{\Delta\omega_{\mathrm{r}}} - \sin\theta_s\cos\theta_s\frac{\Delta i_{ds}}{\Delta\omega_{\mathrm{r}}}) \\ &\quad - cos^2\theta_s \mathrm{r}_1\frac{\Delta\omega_{r-est}}{\Delta\omega_r}(v_{qs} - 2\mathrm{R}_s i_{qs-est} - \omega_{r-est} P\lambda_{af}) \\ &\quad - P i_{qs-est}\lambda_{af}\frac{\Delta\omega_{r-est}}{\Delta\omega_r} \\ &\quad - (\cos\theta_s\frac{\Delta i_{ds}}{\Delta\omega_{\mathrm{r}}} - \sin\theta_s\frac{\Delta i_{qs}}{\Delta\omega_{\mathrm{r}}})v_{ds}\cos\theta_s \\ &\quad + v_{ds}\cos\theta_s\sin\theta_s \mathrm{r}_1\frac{\Delta\omega_{r-est}}{\Delta\omega_r}\end{aligned} \tag{60}$$

$$\begin{aligned}\frac{\Delta\varepsilon}{\Delta\omega_r} &= (v_{qs} - 2\mathrm{R}_s i_{qs-est} - \omega_{r-est} P\lambda_{af}) \\ &\quad \times (\sin^2\theta_s\frac{\Delta i_{qs}}{\Delta\omega_{\mathrm{r}}} - \sin\theta_s\cos\theta_s\frac{\Delta i_{ds}}{\Delta\omega_{\mathrm{r}}}) - v_{ds} \\ &\quad \times (-\cos\theta_s\sin\theta_s\frac{\Delta i_{qs}}{\Delta\omega_{\mathrm{r}}} + \cos^2\theta_s\frac{\Delta i_{ds}}{\Delta\omega_{\mathrm{r}}}) \\ &\quad + (v_{ds}\cos\theta_s\sin\theta_s \mathrm{r}_1 - cos^2\theta_s \mathrm{r}_1(v_{qs} - 2\mathrm{R}_s i_{qs-est} \\ &\quad - \omega_{r-est} P\lambda_{af}) - P i_{qs-est}\lambda_{af})\frac{\Delta\omega_{r-est}}{\Delta\omega_r}\end{aligned} \tag{61}$$

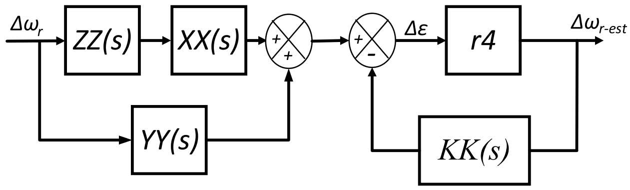

FIGURE 4. Closed-loop representation of Y-MRAS speed estimator for single current sensor-based speed sensorless vector controlled PMSM drive.

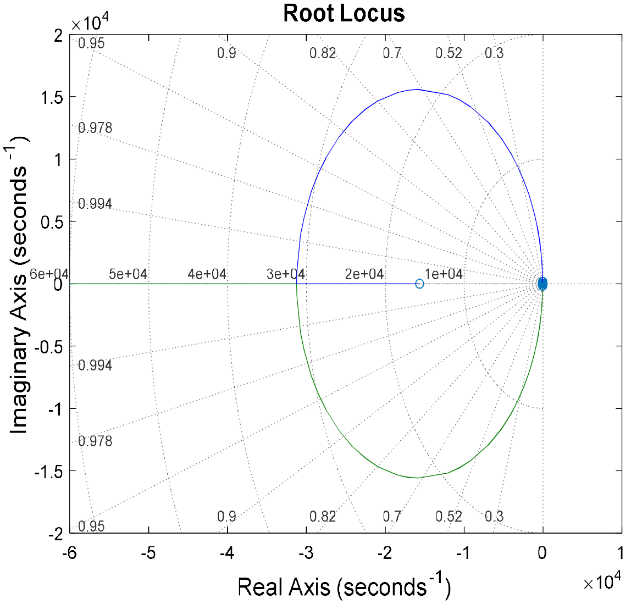

FIGURE 5. Root Locus of Y-MRAS speed estimator with the single current sensor in motoring mode ($\omega_r = 75\,\frac{rad}{sec}, T = 7N.m$).

From the Y-$MRAS$ adaption mechanism, from (24) and (31)

$$\Delta\omega_{r-est} = r_4 * \Delta\varepsilon \tag{62}$$

$$\Delta\varepsilon = \frac{\Delta\omega_{r-est}}{r_4} \tag{63}$$

Substituting $\Delta\varepsilon$ (i.e., (63)) in (61), we obtain

$$\begin{aligned}
&\frac{\Delta\omega_{r-est}}{r_4\Delta\omega_r} \\
&= \left(v_{qs} - 2R_s i_{qs-est} - \omega_{r-est}P\lambda_{af}\right) \\
&\quad \times \left(\sin^2\theta_s\frac{\Delta i_{qs}}{\Delta\omega_r} - \sin\theta_s\cos\theta_s\frac{\Delta i_{ds}}{\Delta\omega_r}\right) \\
&\quad - v_{ds}\left(-\cos\theta_s\sin\theta_s\frac{\Delta i_{qs}}{\Delta\omega_r} + \cos^2\theta_s\frac{\Delta i_{ds}}{\Delta\omega_r}\right) \\
&\quad + (v_{ds}\cos\theta_s\sin\theta_s r_1 - \left(v_{qs} - 2R_s i_{qs-est} - \omega_{r-est}P\lambda_{af}\right) \\
&\quad \times cos^2\theta_s r_1 - Pi_{qs-est}\lambda_{af})\frac{\Delta\omega_{r-est}}{\Delta\omega_r}
\end{aligned} \tag{64}$$

The Closed-loop representation of Y-$MRAS$-based speed-estimation for a single current sensor-based vector controlled PMSM drive is shown in Fig. 4 for (72). Fig. 5 and Fig. 6 show the root Locus for motoring and regenerating modes

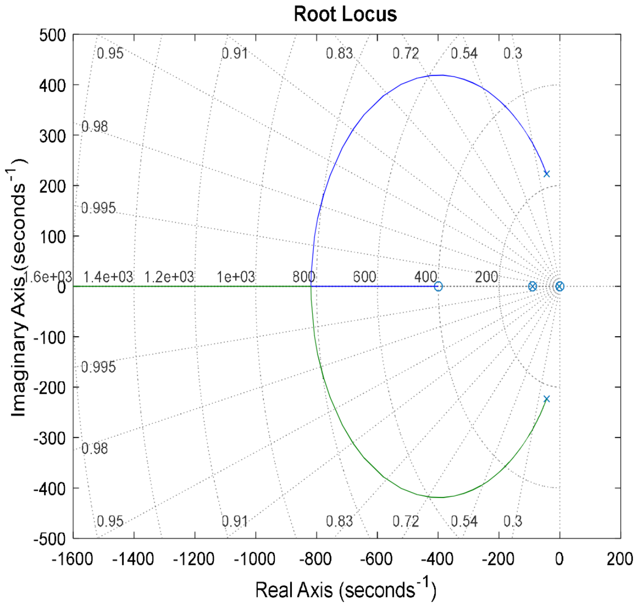

FIGURE 6. Root Locus of Y-MRAS speed estimator with the single current sensor in regenerating mode ($\omega_r = -75\,\frac{rad}{sec}, T = 7N.m$).

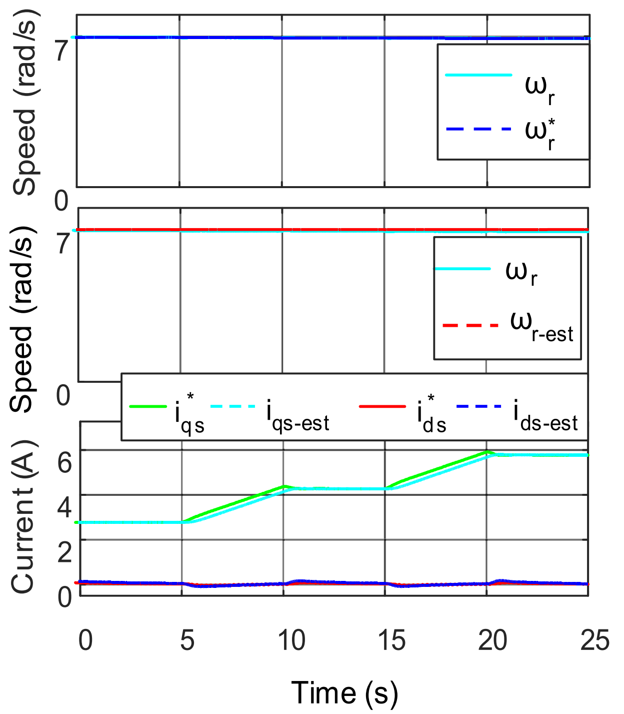

FIGURE 7. Simulation results for the various load.

for one operating point.

$$\begin{aligned}
&\frac{\Delta\omega_{r-est}}{r_4\Delta\omega_r} \\
&\quad - \left(v_{ds}\cos\theta_s\sin\theta_s r_1 - \left(v_{qs} - 2R_s i_{qs-est} - \omega_{r-est}P\lambda_{af}\right)\right. \\
&\quad \left.\times cos^2\theta_s r_1 - Pi_{qs-est}\lambda_{af}\right)\frac{\Delta\omega_{r-est}}{\Delta\omega_r} \\
&= \left(v_{qs} - 2R_s i_{qs-est} - \omega_{r-est}P\lambda_{af}\right)
\end{aligned}$$

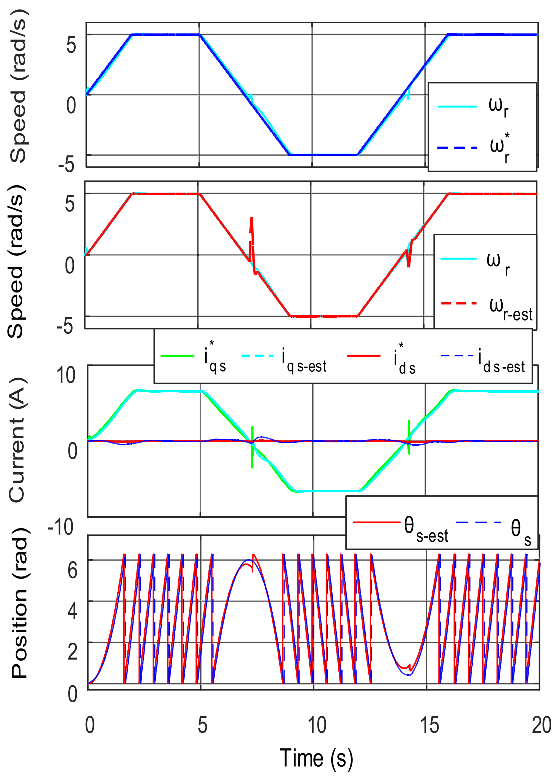

FIGURE 8. Simulation results for ramp speed command.

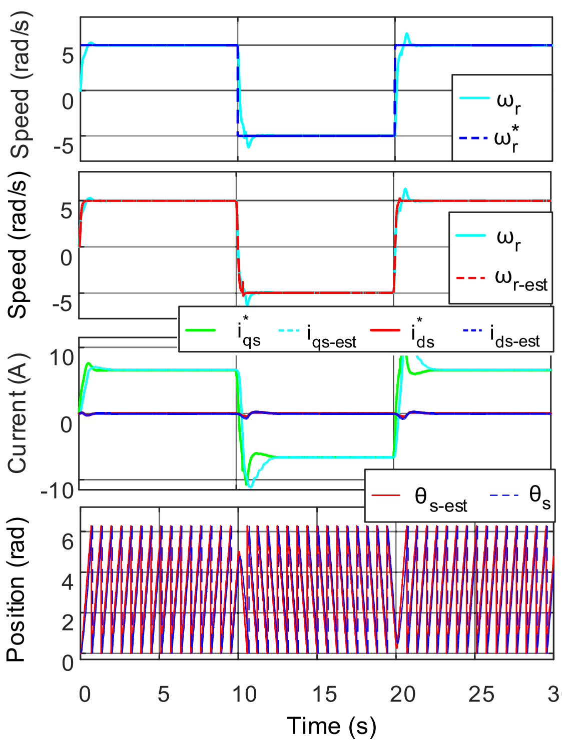

FIGURE 9. Simulation results for step-speed command.

$$\times\left(-\sin\theta_s\cos\theta_s\frac{\Delta i_{ds}}{\Delta\omega_r}+\sin^2\theta_s\frac{\Delta i_{qs}}{\Delta\omega_r}\right)$$
$$-v_{ds}\left(\cos^2\theta_s\frac{\Delta i_{ds}}{\Delta\omega_r}-\cos\theta_s\sin\theta_s\frac{\Delta i_{qs}}{\Delta\omega_r}\right) \tag{65}$$

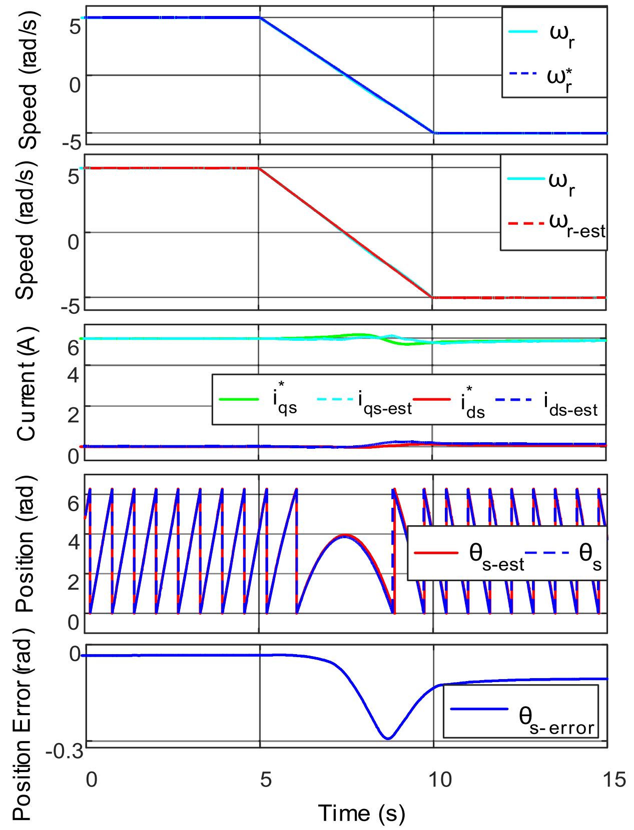

FIGURE 10. Simulation results for regeneration mode.

$$\frac{\Delta\omega_{r-est}}{\Delta\omega_r}$$
$$\times\left\{1-r_4\left(v_{ds}\cos\theta_s\sin\theta_s \mathrm{r}_1-\left(v_{qs}-2R_s i_{qs-est}\right.\right.\right.$$
$$\left.\left.\left.-\omega_{r-est}P\lambda_{af}\right)cos^2\theta_s \mathrm{r}_1-Pi_{qs-est}\lambda_{af}\right)\right\}$$
$$=r_4\left(-2R_s i_{qs-est}+v_{qs}-\omega_{r-est}P\lambda_{af}\right)$$
$$*\,(-\sin\theta_s\cos\theta_s\frac{\Delta i_{ds}}{\Delta\omega_r}+\sin^2\theta_s\frac{\Delta i_{qs}}{\Delta\omega_r})$$
$$-v_{ds}(\cos^2\theta_s\frac{\Delta i_{ds}}{\Delta\omega_r}-\cos\theta_s\sin\theta_s\frac{\Delta i_{qs}}{\Delta\omega_r})\} \tag{66}$$

Let,

$$ZZ(s)$$
$$=\left(v_{qs}-2R_s i_{qs-est}-\omega_{r-est}P\lambda_{af}\right) \tag{67}$$
$$XX\ (s)$$
$$=\left(-\sin\theta_s\cos\theta_s\frac{\Delta i_{ds}}{\Delta\omega_r}+\sin^2\theta_s\frac{\Delta i_{qs}}{\Delta\omega_r}\right) \tag{68}$$
$$YY\ (s)$$
$$=-v_{ds}\left(\cos^2\theta_s\frac{\Delta i_{ds}}{\Delta\omega_r}-\cos\theta_s\sin\theta_s\frac{\Delta i_{qs}}{\Delta\omega_r}\right) \tag{69}$$
$$KK\ (s)$$
$$=-\left(v_{ds}\cos\theta_s\sin\theta_s \mathrm{r}_1-(v_{qs}-2R_s i_{qs-est}-\omega_{r-est}P\lambda_{af})\right.$$
$$\left.\times cos^2\theta_s \mathrm{r}_1-Pi_{qs-est}\lambda_{af}\right) \tag{70}$$

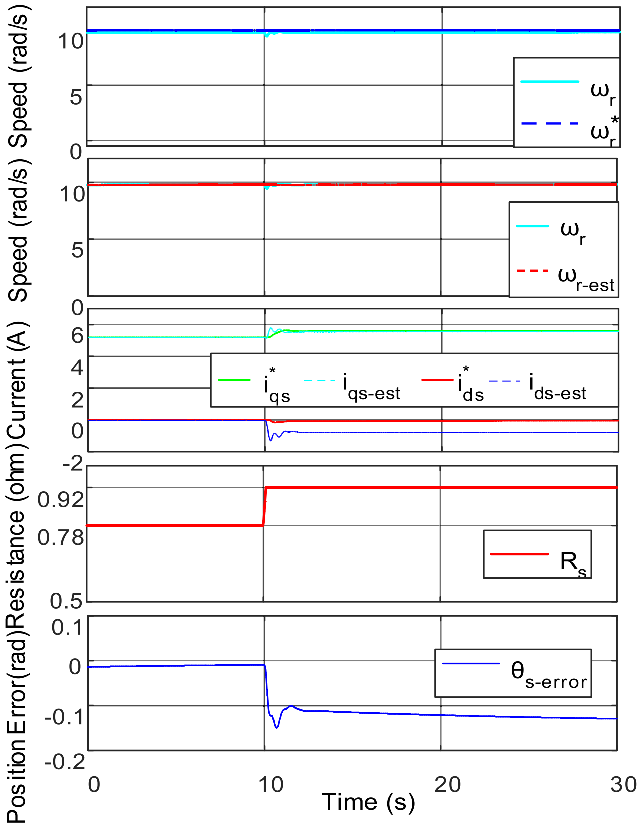

FIGURE 11. Simulation results for stator resistance variation.

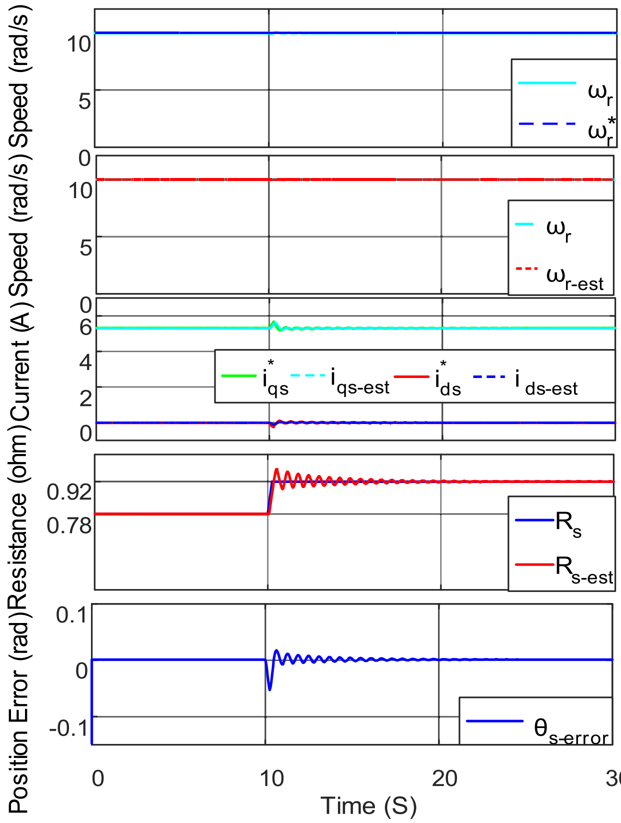

FIGURE 12. Simulation results for stator resistance variation and its compensation.

$$\frac{\Delta\omega_{r-est}}{\Delta\omega_r}1 + r_4KK(s)\} = r_4ZZ\,(s)\,XX\,(s) + YY(s)\} \quad (71)$$

We get

$$\frac{\Delta\omega_{r-est}}{\Delta\omega_r} = \frac{r_4\,\{ZZ\,(s)\,XX\,(s) + YY\,(s)\}}{\{1 + r_4KK\,(s)\}} \quad (72)$$

V. SIMULATION RESULTS

Block diagram for PMSM drive without position, speed, and a current sensor is shown in Fig. 3. The presented drive in Fig. 3 is developed in MATLAB/SIMULINK platform. The simulation performance for various operating conditions is presented in Fig. 7 to Fig. 12. Machine parameters are presented in Table 1. The actual shaft speed (ω_r) is plotted on the same scale with reference (ω_{ref}) and estimated ($\omega_{\text{r-est}}$) speed. The estimated ($i_{qs-est}\&i_{ds-est}$) and reference ($i_{qs}^*\&i_{ds}^*$) currents are plotted on the same scale to demonstrate the accuracy of the estimation quantities.

A. VARIOUS STEP LOAD

In Fig. 7, simulation-results are shown for constant speed with variable loaded conditions. The reference speed (ω_{ref}) is set at 7 rad/s, and the load is changed in ramp form: from t = 5 s to 10 s and t = 15 s to 20 s. The ω_r is plotted on the same scale with ω_r^* and ω_{r-est} speed. Reference current ($i_{qs}^*\&i_{ds}^*$) and estimated ($i_{qs-est}\&i_{ds-est}$) currents are plotted on the same scale.

B. RAMP RESPONSE

The presented algorithm is verified for PMSM drive for a ramp type ω_r^* for reverse and forward motoring of PMSM drive with a constant- Speed/Torque load ("$k\omega_r load$") and the simulation results are presented in Fig. 8. The motor reference speed is changed from 5 rad/s to -5 rad/s in ramp form. The simulation results confirm the estimation technique performance (i.e., speed sensorless and single current sensor).

C. STEP RESPONSE

The step response for the presented speed sensorless with a single current sensor algorithm is verified and presented in Fig. 9 for the PMSM drive. The ω_r^* is altered between ±5 rad/s at 10 s and 20 s. The ω_r is plotted with ω_r^* and ω_{r-est}. The estimated and reference currents are plotted on the same graph to demonstrate the performance of the estimating method.

D. REGENERATIVE MODE

The speed sensorless with a single-current sensor algorithm is verified for regenerative mode, and the results are presented in Fig. 10. The speed is changed in a slow zero-crossing ramp form: i.e., +5 rad/s to -5 rad/s from 5 s to 10 s. first and fourth quadrant operation is performed with a speed of

TABLE 1. Machine parameters.

"Nominal Shaft Power" (P_N)	3 KW
"Pole-pair" (P)	2
"Nominal-speed" (ω_n)	157 rad/s.
"$d-axis$ inductance" (L_d)	0.0107637 H
"$q-axis$ inductance" (L_q)	0.0553733 H
λ_{af} ("Mutual flux linkage between rotor and stator due to permanent magnet")	0.553161 Wb/m^2
"Stator resistance" (R_s)	0.78 Ω
Rated Current	5.9 A
Rated Voltage	415 V
Rated Torque	16 N.m

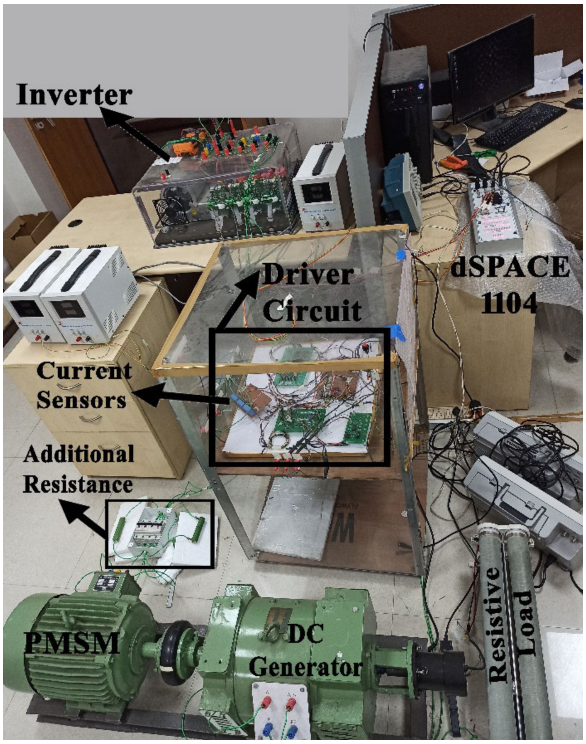

FIGURE 13. Experimental setup.

$\pm 5 rad/s$, and torque producing component is $i_{qs} = 6A$. The simulation results confirm the satisfactory performance for a regenerative mode of operation.

E. STATOR RESISTANCE VARIATION AND COMPENSATION

Figure 11 shows the speed-sensorless response with a single current sensor algorithm for stator resistance variation, and Fig. 12 shows the simulation results with online stator resistance compensation. R_s is varied from 0.78 ohms to 0.92 ohms in a sudden ramp form in 1 sec, the speed and load are maintained constant with 10 rad/s and 8.8 Nm, respectively. Under mathrmR_s variation, vector control is lost ($i_d \neq 0$) and at very low speeds, the drive may go unstable [47]. So, to overcome this, we need an online R_s estimation technique for estimation and compensation. Online stator resistance estimation is done using [18], independent of speed, and the speed estimation algorithm is compensated. Three estimation algorithms are used to robust drive performance against stator resistance variation.

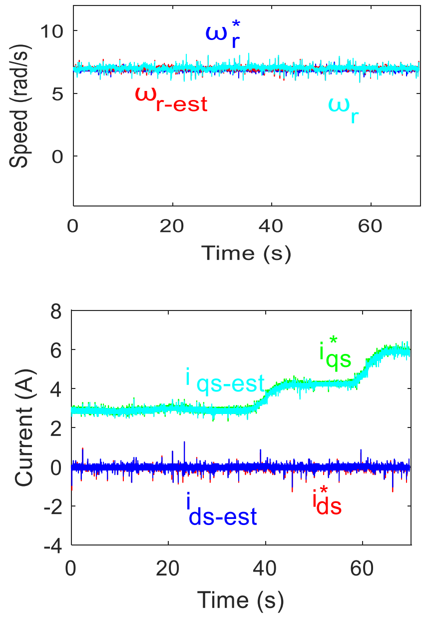

FIGURE 14. Experimental results for change in load at a constant speed.

VI. EXPERIMENTAL VALIDATION

The presented speed sensorless with a single current sensor PMSM drive is verified experimentally using the dSPACE-1104 controller-based PMSM drive (Fig. 13). Laboratory prototype contains PMSM, inverter (IGBT Switches are used in the inverter (IGBT switches SKM75GB12T4), a driver circuit, and dSPACE-1104. The inverter switching frequency is 10 kHz, and 20 kHz discretion frequency. However, no line current filters are required for implementing the proposed drive. The experimental results are performed for various speed/load operating conditions and presented in Fig. 14 to Fig. 18 correspond to the simulation results shown in Fig. 7 to Fig. 10, and Fig. 12.

A. VARIOUS LOADED CONDITION

The drive is verified for various loads under constant speed operation; drive performance is shown in Fig. 14. The load on the machine is changed in a ramp form and maintained constant. $i_{ds} = 0$ is maintained under various operating condition and i_{qs} shows the torque-producing current component.

B. RAMP RESPONSE: REVERSE AND FORWARD MOTORING

The performance of the presented algorithm for the PMSM drive is verified for the ramp speed command, and the drive performance is shown in Fig. 15. The actual speed and ω_{r-est} follow ω_r^*, which confirms the presented algorithm's tracking performance with a single current sensor. Phase voltage and phase currents are shown in Fig. 15.

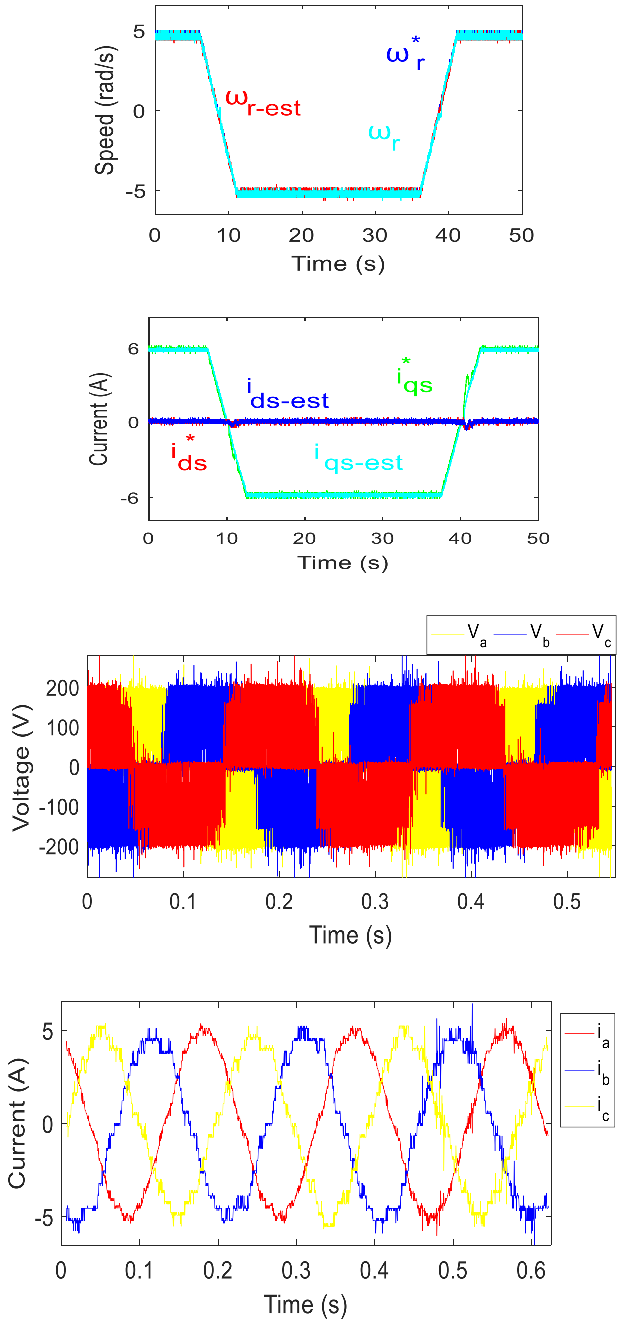

FIGURE 15. **Experimental results for ramp speed command.**

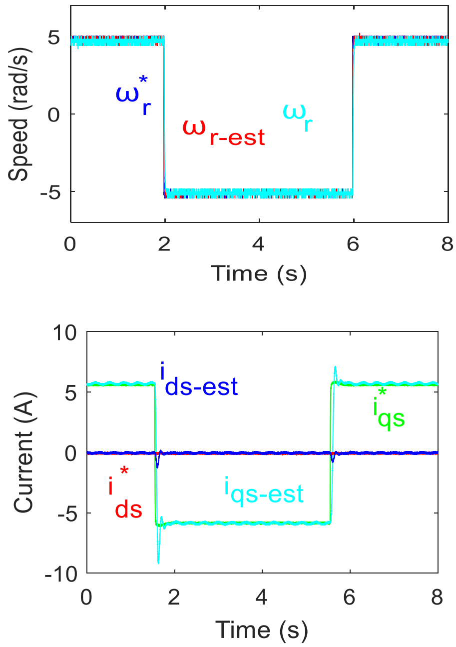

FIGURE 16. **Experimental results for step speed command.**

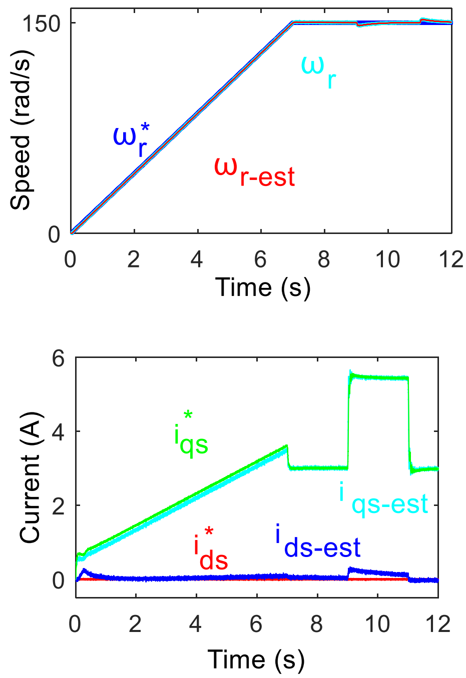

FIGURE 17. **Experimental results for Nominal speed.**

C. STEP RESPONSE: FORWARD AND REVERSE MOTORING

For a step speed command, the machine's performance is tested in both forward and backward modes, and the results are shown in Fig. 16. Reference speed is changed In a step type between ±5 rad/s. ω_r and ω_{r-est}, and ω_r^* are all used to evaluate the drive's performance. To demonstrate the accuracy of the estimation technique, estimated and reference currents are shown on the same scale.

D. NOMINAL SPEED OPERATION

The drive performance is tested for nominal speed, and the corresponding results are present in Fig. 17. Initially, the machine is in the rest position. At 1 sec, the speed command is changed in the ramp form to 150 rad/s. The load acting on the machine is proportional to speed. At t = 8 sec and 10 sec, a sudden load is added and removed. The experimental performance confirms the proposed drive performs satisfactorily under nominal speed operation.

E. STATOR RESISTANCE VARIATION

The drive is verified for change in stator resistance from 0.78 ohms to 0.92 ohms under a constant speed, and the results are

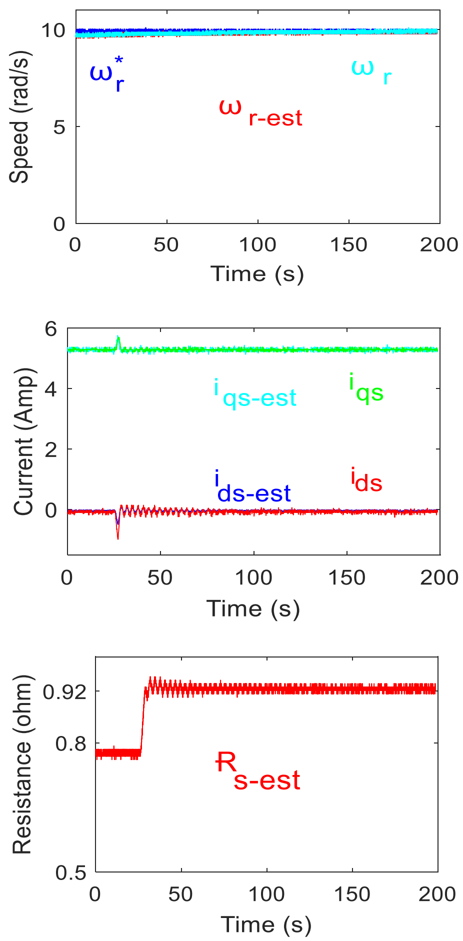

FIGURE 18. Experimental results for change in R_s at constant speed operation.

presented in Fig. 18. The speed and load on the machine are maintained constant. The stator resistance is slowly varied, shown in the estimated stator resistance from Fig. 17. The speed estimation algorithm is closed with the estimated stator resistance. The change in stator resistance will cause minute fluctuation in the system, settled down under a steady state. The experimental results confirm the performance of the present single sensor-based speed sensorless vector control PMSM drive.

F. ZERO SPEED OPERATION

The drive is verified for zero-speed operation, and corresponding results are presented in Fig. 19. Initially, reference speed is maintained at ten rad/s. At t = 20 s and 30 s, reference speed altered between 10 rad/s and 0 rad/s. The load acting on the machine is proportional to speed, as the speed reduced to zero results in zero load on the machine. The experimental result confirms the proposed drive performs satisfactorily under zero-speed operation.

G. COMPARISON BETWEEN THE SINGLE SENSOR AND TWO CURRENT SENSORS PMSM DRIVE

The dynamic performance of the proposed (represented by $\omega_{r-est}, i_{qs-est}$ *and* i_{ds-est}) drive with the existing drive used

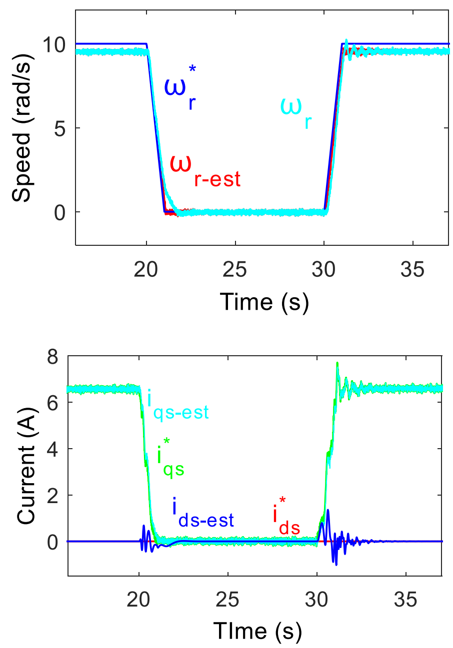

FIGURE 19. Experimental results for zero-speed operation.

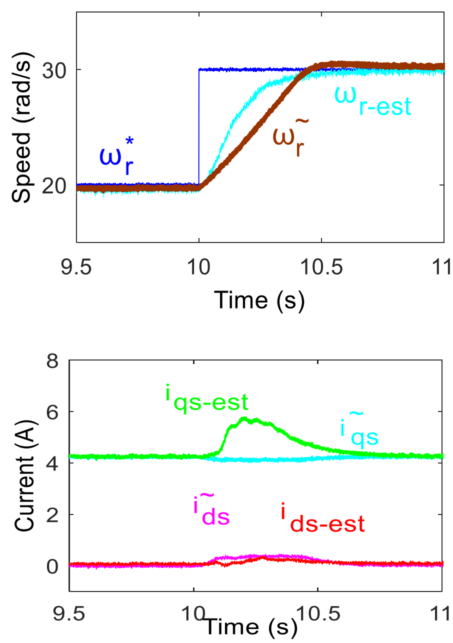

FIGURE 20. Experimental results for two current sensors- and a single current sensor-based speed sensorless vector-control PMSM drive.

two current sensors (represented by $\omega_r^{\sim}, i_{qs}^{\sim}$ *and* $i_{ds}^{\sim}$). It is found that performance is more similar to the existing system shown in Fig. 20. So, this method can also be used in the existing industries where all the sensors are used. As a part of the proposed drive, the authors also clarify that the speed/current estimation techniques can be used to monitor the status of sensors (i.e., speed and current) by implementing them in the existing PMSM drive. No additional hardware is required to implement the proposed single current sensor-based vector-PMSM drive. Implementing a single sensor-based drive can reduce the cost of the drive and complexity of the system as only one current sensor is used and increases the reliability and immunity to signal noise.

VII. CONCLUSION

A single current sensor-based speed sensorless vector controlled PMSM drive is presented in this paper, with speed and current estimation using a single sensor in the drive. The proposed current estimation technique is independent of inverter switching states and machine parameters. The current estimation technique uses the i_{qs}^*, i_{ds}^* and single-phase current information from 3-phase PMSM. PMSM drive speed is estimated using a Y-MRAS-based approach. The speed estimator depends on stator resistance, and thus any variation in it will affect the drive's performance. Here, stator resistance is estimated and compensated online using a modified P-MRAS-based stator resistance estimation technique. It is to be noted that instead of Y-MRAS, any other speed estimation technique can be used, which is independent of stator resistance. The single current sensor-based PMSM drive independent of stator resistance reduces the drive complexity. The speed/current estimation techniques can be used to monitor the status of sensors (i.e., speed and current) by implementing them in the existing PMSM drive. A single current sensor is employed to perform the drive operation with speed and current estimation techniques. Cost and complexity are reduced in the drive. Reliability and immunity to signal noise are increased. The proposed drive is independent of switching states, integrator, and differentiator terms. The proposed drive is simulated in MATLAB/SIMULINK and verified on the Hardware setup developed in the laboratory. The experimental results are consistent with the simulation, confirming the utility of the suggested low-cost approach. The stability of the proposed drive is reported for motoring and regenerating mode.

ACKNOWLEDGMENT

Princess Nourah bint Abdulrahman University Researchers Supporting Project Number (PNURSP2023R79), Princess Nourah bint Abdulrahman University, Riyadh, Saudi Arabia.

REFERENCES

[1] R. Krishnan, *Permanent Magnet Synchronous and Brushless DC Motor Drives*. Boca Raton, FL, USA: CRC Press, 2017.

[2] B. K. Bose, *Modern Power Electronics and AC Drives*. Upper Saddle River, NJ, USA: Prentice-Hall, 2002.

[3] D.-W. Chung and S.-K. Sul, "Analysis and compensation of current measurement error in vector-controlled AC motor drives," *IEEE Trans. Ind. Appl.*, vol. 34, no. 2, pp. 340–345, Mar. 1998, doi: 10.1109/28.663477.

[4] X. Song, B. Han, S. Zheng, and S. Chen, "A novel sensorless rotor position detection method for high-speed surface PM motors in a wide speed range," *IEEE Trans. Power Electron.*, vol. 33, no. 8, pp. 7083–7093, Aug. 2018, doi: 10.1109/TPEL.2017.2753289.

[5] P. L. Xu and Z. Q. Zhu, "Novel square-wave signal injection method using zero-sequence voltage for sensorless control of PMSM drives," *IEEE Trans. Ind. Electron.*, vol. 63, no. 12, pp. 7444–7454, Dec. 2016, doi: 10.1109/TIE.2016.2593657.

[6] C. Lascu and G.-D. Andreescu, "PLL position and speed observer with integrated current observer for sensorless PMSM drives," *IEEE Trans. Ind. Electron.*, vol. 67, no. 7, pp. 5990–5999, Jul. 2020, doi: 10.1109/TIE.2020.2972434.

[7] G. Wang, J. Kuang, N. Zhao, G. Zhang, and D. Xu, "Rotor position estimation of PMSM in low-speed region and standstill using zero-voltage vector injection," *IEEE Trans. Power Electron.*, vol. 33, no. 9, pp. 7948–7958, Sep. 2018, doi: 10.1109/TPEL.2017.2767294.

[8] S. S. Badini, C. D. Kumar, and V. Verma, "Single sensor based vector controlled PMSM drive," in *Proc. IEEE Int. Conf. Power Electron., Drives Energy Syst. (PEDES)*, Dec. 2020, pp. 1–5, doi: 10.1109/PEDES49360.2020.9379428.

[9] S. S. Badini, C. D. Kumar, and V. Verma, "Speed sensorless vector controlled PMSM drive with a single current sensor," in *Proc. IEEE Int. Conf. Power Electron., Drives Energy Syst. (PEDES)*, Dec. 2020, pp. 1–6, doi: 10.1109/PEDES49360.2020.9379614.

[10] Y. Xu, H. Yan, J. Zou, B. Wang, and Y. Li, "Zero voltage vector sampling method for PMSM three-phase current reconstruction using single current sensor," *IEEE Trans. Power Electron.*, vol. 32, no. 5, pp. 3797–3807, Jul. 2017, doi: 10.1109/TPEL.2016.2588141.

[11] M. Carpaneto, P. Fazio, M. Marchesoni, and G. Parodi, "Dynamic performance evaluation of sensorless permanent-magnet synchronous motor drives with reduced current sensors," *IEEE Trans. Ind. Electron.*, vol. 59, no. 12, pp. 4579–4589, Dec. 2012, doi: 10.1109/TIE.2012.2185010.

[12] B. Hafez, A. S. Abdel-Khalik, A. M. Massoud, S. Ahmed, and R. D. Lorenz, "Single-sensor-based three-phase permanent-magnet synchronous motor drive system with Luenberger observers for motor line current reconstruction," *IEEE Trans. Ind. Appl.*, vol. 50, no. 4, pp. 2602–2613, Jan. 2014, doi: 10.1109/TIA.2013.2296625.

[13] S.-C. Yang, "Initial rotor position estimation of permanent magnet synchronous machines using square-wave voltage injection with a single current sensor," in *Proc. IEEE Appl. Power Electron. Conf. Expo.*, Mar. 2014, pp. 2430–2437, doi: 10.1109/APEC.2014.6803644.

[14] S. Nalakath, M. Preindl, and A. Emadi, "Online multi-parameter estimation of interior permanent magnet motor drives with finite control set model predictive control," *IET Electric Power Appl.*, vol. 11, no. 5, pp. 944–951, May 2017, doi: 10.1049/iet-epa.2016.0514.

[15] S. Xiao, T. Shi, X. Li, Z. Wang, and C. Xia, "Single-current-sensor control for PMSM driven by quasi-Z-source inverter," *IEEE Trans. Power Electron.*, vol. 34, no. 7, pp. 7013–7024, Jul. 2019, doi: 10.1109/TPEL.2018.2875533.

[16] P. Kshirsagar and R. Krishnan, "Sensorless control of permanent magnet motors operating at low switching frequency for climate control systems," in *Proc. 3rd IEEE Int. Symp. Sensorless Control Electr. Drives (SLED)*, Sep. 2012, pp. 1–8, doi: 10.1109/SLED.2012.6422823.

[17] O. C. Kivanc and S. B. Ozturk, "Sensorless PMSM drive based on stator feedforward voltage estimation improved with MRAS multiparameter estimation," *IEEE/ASME Trans. Mechatronics*, vol. 23, no. 3, pp. 1326–1337, Jun. 2018, doi: 10.1109/TMECH.2018.2817246.

[18] S. S. Badini and V. Verma, "A new stator resistance estimation technique for vector-controlled PMSM drive," *IEEE Trans. Ind. Appl.*, vol. 56, no. 6, pp. 6536–6545, Nov. 2020, doi: 10.1109/TIA.2020.3025265.

[19] M. S. Rafaq, F. Mwasilu, J. Kim, H. H. Choi, and J.-W. Jung, "Online parameter identification for model-based sensorless control of interior permanent magnet synchronous machine," *IEEE Trans. Power Electron.*, vol. 32, no. 6, pp. 4631–4643, Jun. 2017, doi: 10.1109/TPEL.2016.2598731.

[20] R. Tami, D. Boutat, G. Zheng, F. Kratz, and R. El Gouri, "Rotor speed, load torque and parameters estimations of a permanent magnet synchronous motor using extended observer forms," *IET Control Theory Appl.*, vol. 11, no. 9, pp. 1485–1492, Jun. 2017, doi: 10.1049/iet-cta.2016.0226.

[21] S. Morimoto, M. Sanada, and Y. Takeda, "High-performance current-sensorless drive for PMSM and SynRM with only low-resolution position sensor," *IEEE Trans. Ind. Appl.*, vol. 39, no. 3, pp. 792–801, May 2003, doi: 10.1109/TIA.2003.811782.

[22] J. I. Ha, "Current prediction in vector-controlled PWM inverters using single DC-link current sensor," *IEEE Trans. Ind. Electron.*, vol. 57, no. 2, pp. 716–726, Feb. 2010, doi: 10.1109/TIE.2009.2028361.

[23] B. Singh and D. Goyal, "Improved DSVM-DTC based current sensorless permanent magnet synchronous motor drive," in *Proc. 7th Int. Conf. Power Electron. Drive Syst.*, Nov. 2007, pp. 1354–1360, doi: 10.1109/PEDS.2007.4487880.

[24] J. Zhao, S. Nalakath, and A. Emadi, "A high frequency injection technique with modified current reconstruction for low-speed sensorless control of IPMSMs with a single DC-link current sensor," *IEEE Access*, vol. 7, pp. 136137–136147, 2019, doi: 10.1109/ACCESS.2019.2942148.

[25] Y.-S. Lai, Y.-K. Lin, and C.-W. Chen, "New hybrid pulsewidth modulation technique to reduce current distortion and extend current reconstruction range for a three-phase inverter using only DC-link sensor," *IEEE Trans. Power Electron.*, vol. 28, no. 3, pp. 1331–1337, Mar. 2013, doi: 10.1109/TPEL.2012.2207406.

[26] Y. Gu, F. Ni, D. Yang, and H. Liu, "Switching-state phase shift method for three-phase-current reconstruction with a single DC-link current sensor," *IEEE Trans. Ind. Electron.*, vol. 58, no. 11, pp. 5186–5194, Mar. 2011, doi: 10.1109/TIE.2011.2123854.

[27] W.-C. Lee, D.-S. Hyun, and T.-K. Lee, "A novel control method for three-phase PWM rectifiers using a single current sensor," *IEEE Trans. Power Electron.*, vol. 15, no. 5, pp. 861–870, Sep. 2000, doi: 10.1109/63.867675.

[28] L. Zhu, F. Chen, B. Li, C. Li, G. Wang, S. Wang, G. Zhang, and D. Xu, "Phase current reconstruction error suppression method for single DC-link shunt PMSM drives at low-speed region," *IEEE Trans. Power Electron.*, vol. 37, no. 6, pp. 7067–7081, Jun. 2022, doi: 10.1109/TPEL.2021.3136610.

[29] W. Wang, H. Yan, Y. Xu, J. Zou, X. Zhang, W. Zhao, G. Buticchi, and C. Gerada, "New three-phase current reconstruction for PMSM drive with hybrid space vector pulsewidth modulation technique," *IEEE Trans. Power Electron.*, vol. 36, no. 1, pp. 662–673, Jan. 2021, doi: 10.1109/TPEL.2020.2997986.

[30] Y. Cho, T. LaBella, and J.-S. Lai, "A three-phase current reconstruction strategy with online current offset compensation using a single current sensor," *IEEE Trans. Ind. Electron.*, vol. 59, no. 7, pp. 2924–2933, Jul. 2012, doi: 10.1109/TIE.2011.2171177.

[31] H. Kim and T. M. Jahns, "Current control for AC motor drives using a single DC-link current sensor and measurement voltage vectors," *IEEE Trans. Ind. Appl.*, vol. 42, no. 6, pp. 1539–1547, Nov. 2006, doi: 10.1109/TIA.2006.882630.

[32] H. Yan, W. Wang, Y. Xu, and J. Zou, "Position sensorless control for PMSM drives with single current sensor," *IEEE Trans. Ind. Electron.*, vol. 70, no. 1, pp. 178–188, Jan. 2023, doi: 10.1109/TIE.2022.3148748.

[33] B. Saritha and P. A. Janakiraman, "Sinusoidal three-phase current reconstruction and control using a DC-link current sensor and a curve-fitting observer," *IEEE Trans. Ind. Electron.*, vol. 54, no. 5, pp. 2657–2664, Oct. 2007, doi: 10.1109/TIE.2007.899842.

[34] Q. Tang, A. Shen, W. Li, P. Luo, M. Chen, and X. He, "Multiple-positions-coupled sampling method for PMSM three-phase current reconstruction with a single current sensor," *IEEE Trans. Power Electron.*, vol. 35, no. 1, pp. 699–708, Jan. 2020, doi: 10.1109/TPEL.2019.2913684.

[35] K. Sun, Q. Wei, L. Huang, and K. Matsuse, "An overmodulation method for PWM-inverter-fed IPMSM drive with single current sensor," *IEEE Trans. Ind. Electron.*, vol. 57, no. 10, pp. 3395–3404, Oct. 2010, doi: 10.1109/TIE.2009.2038336.

[36] T. C. Green and B. W. Williams, "Derivation of motor line-current waveforms from the DC-link current of an inverter," *IEE Proc. B, Electric Power Appl.*, vol. 136, no. 4, pp. 196–204, Jul. 1989, doi: 10.1049/ip-b.1989.0026.

[37] J. T. Boys, "Novel current sensor for PWM AC drives," *IEE Proc. B, Electric Power Appl.*, vol. 135, no. 1, pp. 27–32, Jan. 1988, doi: 10.1049/ip-b.1988.0005.

[38] F. Blaabjerg, J. K. Pedersen, U. Jaeger, and P. Thoegersen, "Single current sensor technique in the DC-link of three-phase PWM-VS inverters. A review and the ultimate solution," in *Proc. Conf. Rec.-IAS Annu. Meeting*, Mar. 1996, pp. 1192–1202, doi: 10.1109/ias.1996.560230.

[39] G. Wang, F. Chen, N. Zhao, Y. Bai, B. Li, S. Liu, and D. Xu, "Current reconstruction considering time-sharing sampling errors for single DC-link shunt motor drives," *IEEE Trans. Power Electron.*, vol. 36, no. 5, pp. 5760–5770, May 2021, doi: 10.1109/TPEL.2020.3029335.

[40] J.-L. Ha, "Voltage injection method for three-phase current reconstruction in PWM inverters using a single sensor," *IEEE Trans. Power Electron.*, vol. 24, no. 3, pp. 767–775, Mar. 2009, doi: 10.1109/TPEL.2008.2009451.

[41] M. O. Sonnaillon, G. Bisheimer, C. De Angelo, J. Solsona, and G. O. Garcia, "Mechanical-sensorless induction motor drive based only on DC-link measurements," *IEE Proc. Electr. Power Appl.*, vol. 153, no. 6, pp. 815–822, 2006, doi: 10.1049/ip-epa:20050552.

[42] Y. Tomigashi, H. Hida, and K. Ueyama, "Voltage vector correction based on a novel coordinate transformation for motor current detection using a single shunt resistor," in *Proc. 13th Eur. Conf. Power Electron. Appl.*, 2009, pp. 1–8. [Online]. Available: https://ieeexplore.ieee.org/document/5279125

[43] D. P. Marcetic and E. M. Adžic, "Improved three-phase current reconstruction for induction motor drives with DC-link shunt," *IEEE Trans. Ind. Electron.*, vol. 57, no. 7, pp. 2454–2462, Jul. 2010, doi: 10.1109/TIE.2009.2035456.

[44] S. N. Vukosavic and A. M. Stankovic, "Sensorless induction motor drive with a single DC-link current sensor and instantaneous active and reactive power feedback," *IEEE Trans. Ind. Electron.*, vol. 48, no. 1, pp. 195–204, Feb. 2001, doi: 10.1109/41.904580.

[45] V. Vimlesh, C. Chandan, M. Suman, and H. Yoichi, "Speed sensorless vector controlled induction motor drive using single current sensor," *IEEE Trans. Energy Convers.*, vol. 28, no. 4, pp. 938–950, Dec. 2013, doi: 10.1109/TEC.2013.2273935.

[46] Q. Teng, H. Cui, J. Duan, J. Zhu, Y. Guo, and G. Lei, "Extended state observer-based vector control for PMSM drive system with single phase current sensor," in *Proc. 20th Int. Conf. Electr. Mach. Syst. (ICEMS)*, Aug. 2017, pp. 1–6, doi: 10.1109/ICEMS.2017.8056536.

[47] S. S. Badini and V. Verma, "MRAS-based speed and parameter estimation for a vector-controlled PMSM drive," *Electrica*, vol. 20, no. 1, pp. 28–40, Feb. 2020, doi: 10.5152/ELECTRICA.2020.19039.

[48] B. S. Shiva, V. Verma, and Y. A. Khan, "Q-MRAS-based speed sensorless permanent magnet synchronous motor drive with adaptive neural network for performance enhancement at low speeds," in *Innovations in Soft Computing and Information Technology*, J. Chattopadhyay, R. Singh, and V. Bhattacherjee, Eds. Singapore: Springer, 2019. [Online]. Available: https://link.springer.com/chapter/10.1007/978-981-13-3185-5_10, doi: 10.1007/978-981-13-3185-5_10.

[49] G. Zhang, G. Wang, and D. Xu, "Saliency-based position sensorless control methods for PMSM drives—A review," *Chin. J. Electr. Eng.*, vol. 3, no. 2, pp. 14–23, Sep. 2019, doi: 10.23919/cjee.2017.8048408.

[50] G. Wang, M. Valla, and J. Solsona, "Position sensorless permanent magnet synchronous machine drives—A review," *IEEE Trans. Ind. Electron.*, vol. 67, no. 7, pp. 5830–5842, Jul. 2020, doi: 10.1109/TIE.2019.2955409.

[51] S. H. Hosseini and M. Tabatabaei, "IPMSM velocity and current control using MTPA based adaptive fractional order sliding mode controller," *Eng. Sci. Technol., Int. J.*, vol. 20, no. 3, pp. 896–908, Jun. 2017, doi: 10.1016/j.jestch.2017.03.008.

[52] P. Borsje, T. F. Chan, Y. K. Wong, and S. L. Ho, "A comparative study of Kalman filtering for sensorless control of a permanent-magnet synchronous motor drive," in *Proc. IEEE Int. Conf. Electric Mach. Drives*, May 2005, pp. 815–822, doi: 10.1109/IEMDC.2005.195816.

[53] A. Pal, S. Das, and A. K. Chattopadhyay, "An improved rotor flux space vector based MRAS for field-oriented control of induction motor drives," *IEEE Trans. Power Electron.*, vol. 33, no. 6, pp. 5131–5141, Jun. 2018, doi: 10.1109/TPEL.2017.2657648.

[54] S. Maiti, C. Chakraborty, and S. Sengupta, "Simulation studies on model reference adaptive controller based speed estimation technique for the vector controlled permanent magnet synchronous motor drive," *Simul. Model. Pract. Theory*, vol. 17, no. 4, pp. 585–596, Apr. 2009, doi: 10.1016/j.simpat.2008.08.017.

[55] D. Xu, B. Wang, G. Zhang, G. Wang, and Y. Yu, "A review of sensorless control methods for AC motor drives," *CES Trans. Electr. Mach. Syst.*, vol. 2, no. 1, pp. 104–115, Mar. 2018, doi: 10.23919/tems.2018.8326456.

[56] M. Zolfaghari, S. A. Taher, and D. V. Munuz, "Neural network-based sensorless direct power control of permanent magnet synchronous motor," *Ain Shams Eng. J.*, vol. 7, no. 2, pp. 729–740, Jun. 2016, doi: 10.1016/j.asej.2016.01.002.

[57] Y. D. Landau, "Adaptive control: The model reference approach," *IEEE Trans. Syst., Man, Cybern.*, vol. SMC-14, no. 1, pp. 169–170, Jan./Feb. 1984, doi: 10.1109/tsmc.1984.6313284.

[58] I. Benlaloui, S. Drid, L. Chrifi-Alaoui, and M. Ouriagli, "Implementation of a new MRAS speed sensorless vector control of induction machine," *IEEE Trans. Energy Convers.*, vol. 30, no. 2, pp. 588–595, Jun. 2014, doi: 10.1109/TEC.2014.2366473.

[59] A. V. R. Teja, C. Chakraborty, S. Maiti, and Y. Hori, "A new model reference adaptive controller for four quadrant vector controlled induction motor drives," *IEEE Trans. Ind. Electron.*, vol. 59, no. 10, pp. 3757–3767, Oct. 2012, doi: 10.1109/TIE.2011.2164769.

[60] A. N. Smith, S. M. Gadoue, and J. W. Finch, "Improved rotor flux estimation at low speeds for torque MRAS-based sensorless induction motor drives," *IEEE Trans. Energy Convers.*, vol. 31, no. 1, pp. 270–282, Mar. 2016, doi: 10.1109/TEC.2015.2480961.

[61] M. Cirrincione, M. Pucci, G. Cirrincione, and G. A. Capolino, "A new TLS-based MRAS speed estimation with adaptive integration for high-performance induction machine drives," *IEEE Trans. Ind. Appl.*, vol. 40, no. 4, pp. 1116–1137, Jul. 2004, doi: 10.1109/TIA.2004.830779.

[62] S. M. Gadoue, D. Giaouris, and J. W. Finch, "Sensorless control of induction motor drives at very low and zero speeds using neural network flux observers," *IEEE Trans. Ind. Electron.*, vol. 56, no. 8, pp. 3029–3039, Aug. 2009, doi: 10.1109/TIE.2009.2024665.

[63] Q. Gao, C. S. Spiteri, G. M. Asher, and M. Sumner, "Sensorless speed operation of cage induction motor using zero drift feedback integration with MRAS observer," in *Proc. Eur. Conf. Power Electron. Appl.*, 2005, p. 9, doi: 10.1109/EPE.2005.219238.
[64] S. Ye, "A novel fuzzy flux sliding-mode observer for the sensorless speed and position tracking of PMSMs," *Optik*, vol. 171, pp. 319–325, Oct. 2018, doi: 10.1016/j.ijleo.2018.06.074.
[65] H. Niu, J. Yu, H. Yu, C. Lin, and L. Zhao, "Adaptive fuzzy output feedback and command filtering error compensation control for permanent magnet synchronous motors in electric vehicle drive systems," *J. Franklin Inst.*, vol. 354, no. 15, pp. 6610–6629, Oct. 2017, doi: 10.1016/j.jfranklin.2017.08.021.
[66] B. S. Shiva and V. Verma, "Speed and parameter estimation of vector controlled permanent magnet synchronous motor drive," in *Proc. 2nd Int. Conf. Power, Energy Environ., Towards Smart Technol. (ICEPE)*, Jun. 2018, pp. 1–6, doi: 10.1109/EPETSG.2018.8658882.
[67] R. Kumar, S. Das, and A. K. Chattopadhyay, "Comparative assessment of two different model reference adaptive system schemes for speed-sensorless control of induction motor drives," *IET Electr. Power Appl.* vol. 10, no. 2, pp. 141–154, 2016.
[68] S. S. Badini and V. Verma, "A novel MRAS based speed sensorless vector controlled PMSM drive," in *Proc. 54th Int. Universities Power Eng. Conf. (UPEC)*, Sep. 2019, pp. 1–6, doi: 10.1109/UPEC.2019.8893607.
[69] A. V. R. Teja and C. Chakraborty, "A novel model reference adaptive controller for estimation of speed and stator resistance for vector controlled induction motor drives," in *Proc. IEEE Int. Symp. Ind. Electron.*, Jul. 2010, pp. 1187–1192, doi: 10.1109/ISIE.2010.5636637.

SAI SHIVA BADINI received the B.Tech. degree in electrical and electronics engineering from Jawaharlal Nehru Technological University Hyderabad, Hyderabad, India, in 2012, the M.Tech. degree in energy systems from the College of Engineering Hyderabad, Jawaharlal Nehru Technological University Hyderabad, in 2015, and the Ph.D. degree in control systems from the National Institute of Technology Patna, Patna, India, in 2022. His current research interests include special machine drives, sensor reduction, power electronics, and renewable energy.

VIMLESH VERMA (Senior Member, IEEE) was born in Mumbai, India. He received the B.Tech. degree in electrical and electronics engineering from Andhra University, Visakhapatnam, India, in 2002, the M.Tech. degree in power apparatus and systems from Nirma University, Ahmedabad, India, in 2005, and the Ph.D. degree in electrical engineering from the Indian Institute of Technology Kharagpur, Kharagpur, India, in 2015. He is currently an Assistant Professor with the Department of Electrical Engineering, National Institute of Technology Patna, Patna, India. His research interests include the sensorless control of AC drives, fault diagnosis, motor drives, power converters, electric vehicles, and renewable energy.

MOHD TARIQ (Senior Member, IEEE) received the B.Tech. degree in electrical engineering from Aligarh Muslim University (AMU), Aligarh, the M.Tech. degree in machine drives and power electronics from the Indian Institute of Technology (IIT) Kharagpur, and the Ph.D. degree in electrical engineering with a focus on power electronics and control from Nanyang Technological University (NTU), Singapore.

He was an Assistant Professor with the Maulana Azad National Institute of Technology (MANIT), Bhopal, India. He is currently a Faculty/Postdoctoral Associate with Florida International University, where he is associated with the Energy, Power, Sustainability, and Intelligence (EPSi) Group and working on high penetration renewable systems, grid resiliency, large-scale data analysis, artificial intelligence, electric vehicle, and cybersecurity. He is also an Assistant Professor (on leave) with AMU, where he was directing various internationally and nationally sponsored research projects and led a team of multiple researchers in the domain of power converters, energy storage devices, and their optimal control for electrified transportation and renewable energy application. He has secured several fundings worth approximately 18 million INR for AMU. Previously, he has worked as a Researcher at the Rolls-Royce-NTU Corporate Laboratory, Singapore, where he has worked on the design and development of power converters for more electric aircraft. Before joining the Ph.D. degree, he was a Scientist with the National Institute of Ocean Technology, Chennai, under the Ministry of Earth Sciences, Government of India, where he worked on the design and development of BLDC motors for underwater remotely operated vehicle applications. He has authored more than 225 research papers in international journals/conferences, including many articles in IEEE TRANSACTIONS/journals. He is also an inventor of more than 25 patents granted/published by the patent offices of the USA, Australia, the U.K., Europe, India, and China.

Dr. Tariq was a recipient of the 2019 Premium Award for Best Paper in *IET Electrical Systems in Transportation* journal for his work on more electric aircraft and also the Best Paper Award from the IEEE Industry Applications Society's (IAS) and the Industrial Electronic Society (IES), Malaysia Section—Annual Symposium (ISCAIE-2016) held in Penang, Malaysia, and many other best paper awards from different international conferences. He is a Young Scientist Scheme Awardee, in 2019, supported by the Department of Science and Technology, Government of India, the Young Engineer Awardee, in 2020, by the Institution of Engineers (India), and the Young Researchers Awardee by the Innovation Council, AMU, in 2021. He is also the Founder Chair of the IEEE AMU Student Branch and the Founder Chair of IEEE SIGHT AMU. He is an Associate Editor of IEEE ACCESS, an Editorial Board Member of *Scientific Report* and *Nature* journal, and a guest editor of various other journals.

SHABANA UROOJ (Senior Member, IEEE) received the B.E. degree in electrical engineering and the M.Tech. degree in instrumentation and control from Aligarh Muslim University, Aligarh, India, in 1998 and 2003, respectively, and the Ph.D. degree from the Department of Electrical Engineering, Jamia Millia Islamia (a central university), Delhi, India, in 2011. She has nearly three years of industry experience and over 19 years of teaching experience. She is currently an Associate Professor with the Department of Electrical Engineering, College of Engineering, Princess Nourah Bint Abdulrahman University, Riyadh, Saudi Arabia. She has guided several Ph.D. and master's theses and dissertations. She has authored or coauthored more than 150 research papers which are published in high-quality international journals and conference proceedings. She was a recipient of the Research Excellence Award from PNU, Springer's Excellence in Teaching and Research Award, the American Ceramic Society's Young Professional Award, the IEEE Region 10 Award for Outstanding Contribution in Educational Activities, and several best paper presentation awards. Recently, she received the Badge of IEEE STEM Ambassador for her excellent volunteering and efforts in STEM promotional activities. She is holding the responsibility of the Vice Chair of the IEEE Saudi Arabia Section.